Improvement of the efficiency in inverted mixed halide perovskite solar cells by PCDTBT doping

Hanadi Mehdi[1,2,*] , Asya Mhamdi[1], Hassen Dhifaoui[1], Muriel Matheron[2], Stéphane Cros[2], and Abdelaziz Bouazizi[1]

[1] *Équipe Dispositifs Électroniques Organiques et Photovoltaïque Moléculaire, Laboratoire de la Matière Condensée et des Nanosciences, Faculté des Sciences de Monastir, Université de Monastir, Avenue de l'environnement, 5019 Monastir, Tunisia*

[2] *Université Grenoble Alpes, CEA, LITEN, INES, 73375 Le Bourget-du-Lac, France*

ABSTRACT

Perovskite solar cells (PSC) have shown extraordinary progress over the last few years with remarkable efficiency. The perovskite film quality and structure can affect the performance of the resulting devices. Herein, the effect of PCDTBT addition on perovskite $MAPbI_{3-x}Cl_x$ precursor solutions on the photovoltaic properties was investigated. It was found that the addition of the PCDTBT has effectively enhanced the efficiencies of the devices. This behavior would be due to the improvement of the $MAPbI_{3-x}Cl_x$ film crystallinity and to the reduction of the recombination pathways due to the passivation of the trap states of the perovskite layer.

1 Introduction

Hybrid organic-inorganic perovskite solar cells (PSC) have attracted considerable interest in the photovoltaic research due to their pleasing properties, including broadband light absorption, high absorption coefficient, adjustable and direct band gap, exciton binding energy, ambipolar charge transport, length diffusion of charge carriers and specially their simple solution fabrication process using low-cost materials [1–6]. Their power conversion efficiency (PCE) has been improved over the last years, increasing from 3.9 to 25.2% [7, 8]. In order to go beyond the current world record, more efforts need to been done to understand the processes behind and to wisely improve the absorber layer and the corresponding architecture of the solar cell (SC).

Optimization of the structure of devices as well as the one of perovskite film deposition methodology are the two important factors for getting SCs with good conversion efficiency. In this context, many efforts and methods have been developed on different components of PSCs to improve photovoltaic performance, including the use of various organic and inorganic hole transport materials [9, 10], elaboration of deposition processes [11, 12], optimization of electron transport layer thickness [13], application of different treatments [14, 15] and optimization of the perovskite structure [16].

https://doi.org/10.1007/s10854-020-04768-8

The structure and composition of the perovskite is one of the important parameters that can influence the performance of perovskite solar cells. Cesium and rubidium cations were added in perovskite structure to improve the stability of the cells [17]. Mixed-cation perovskite solar cells based on $Cs_{0.17}FA_{0.83}Pb$ $(Br_{0.4}I_{0.6})_3$ with an efficiency of 17% were reported [18]. Thus, the doping of the cation sites has considerably improved the photovoltaic performances as well as the stability, while the use of two halogens had a positive impact on transport properties. Among all mixed halide perovskite films, the mixed halide containing I and Cl in MA perovskite-based ($MAPbI_{3-x}Cl_x$) has attracted deductive attention due to its long carrier diffusion length [19, 20].

However, some problems still prevent the perovskite solar cells to reach higher values of PCE due to the diffusion lengths of the electrons and the corresponding holes, as well as due to the uncontrollable crystalline quality of the perovskite film. To overcome these difficulties, various methods involving interface modification as well as doping of perovskite material with an organic material have been developed. Therefore, the poly [N- 9′-heptadecanyl-2,7-carbazole-alt-5,5-(4,7-di-2-thienyl-2′,1′,3′-benzothiadiazole] (PCDTBT) was found to be a good doping material. In fact, it is a hole transport material, generally used in organic polymer solar cells. Its highest level of molecular orbital energy (HOMO) is in order of 5.45 eV [21], corresponding well with the one of $MAPbI_{3-x}Cl_x$ (5.4 eV). It also presents a broad absorption in the visible range. The repeating unit of PCDTBT possesses lone electron pairs attached to its S and N atoms, which can effectively passivate the under-coordinated Pb ions in the perovskite film.

In this paper, we developed a planar inverted solar cell based on mixed halide perovskite $MAPbI_{3-x}Cl_x$. The effects of PCDTBT additive to the $MAPbI_{3-x}Cl_x$ perovskite films on the performance of the cells were investigated.

2 Experimental section

2.1 Solar cell fabrication

Solar cell devices were fabricated on Indium tin oxide (ITO)-coated glass. After laser graving, the patterned ITO glass (resistance 15 Ω sq.$^{-1}$) was cleaned by ultrasonication sequentially in acetone, isopropyl and deionized water for 10 min. The PEDOT:PSS layer was deposited on the cleaned substrate through spin-coating at 4000 rpm for 40 s, followed by annealing treatment at 180 °C for 1 h. Afterward, a blend perovskite precursor solutions of methylammonium iodide and lead (II) chloride were dissolved in N,Ndimethylformamide (DMF) at a 3:1 M ratio, respectively, for MAI: $PbCl_2$ with and without the addition of the PCDTBT(0.2 mg.ml^{-1}) and then stirred at room temperature overnight in glove box. After that, the perovskite solution was used to spin-coat the PEDOT:PSS surface at 4000 rpm for 40 s. The perovskite films were then heated at 100 °C for 30 min. After the thermal annealing of the perovskite layer, the electron transport material $PC_{60}BM$ ([6,6]-phenyl-C60-butyric acid methyl ester) (30 mg/ml in Chlorobenzene) was deposited on the top of perovskite film by spin-coating at 1500 rpm for 60 s. The whole fabrication process was completed after the thermal evaporation of a 8 nm BCP(Bathocuproine – 2,9-Dimethyl-4,7-diphenyl-1,10-phenanthroline) and 100 nm Ag on top of the $PC_{60}BM$ layer.

The schematic illustration of the planar inverted perovskite solar cell with the structure ITO/PEDOT:PSS/$CH_3NH_3PbI_{3-x}Cl_x$:PCDTBT/$PC_{60}BM$/BCP/ Ag is shown in Fig. 1.

2.2 Characterization

The X-ray diffraction (XRD) patterns of the thin films were measured by a Siemens D5000 diffractometer using Cu Kα radiation (λ = 1.54 Å). The UV–Vis spectra were collected using a PerkinElmer Instruments, Lamda 35 spectrophotometer. The surface morphologies were inspected by scanning electron microscopy (SEM, LEO 1530). Photoluminescence spectra have been recorded using a Perkin Elmer Lambda 35 spectrophotometer. Photoluminescence spectra have been performed with a "Jobin Yvon-Spex Spectrum One" CCD detector, cooled at liquid nitrogen temperature. The current–voltage characteristics under illumination AM 1.5 G (100 mW.cm − 2) with Xe Oriel solar simulator were obtained with a Keithley 2402 source.
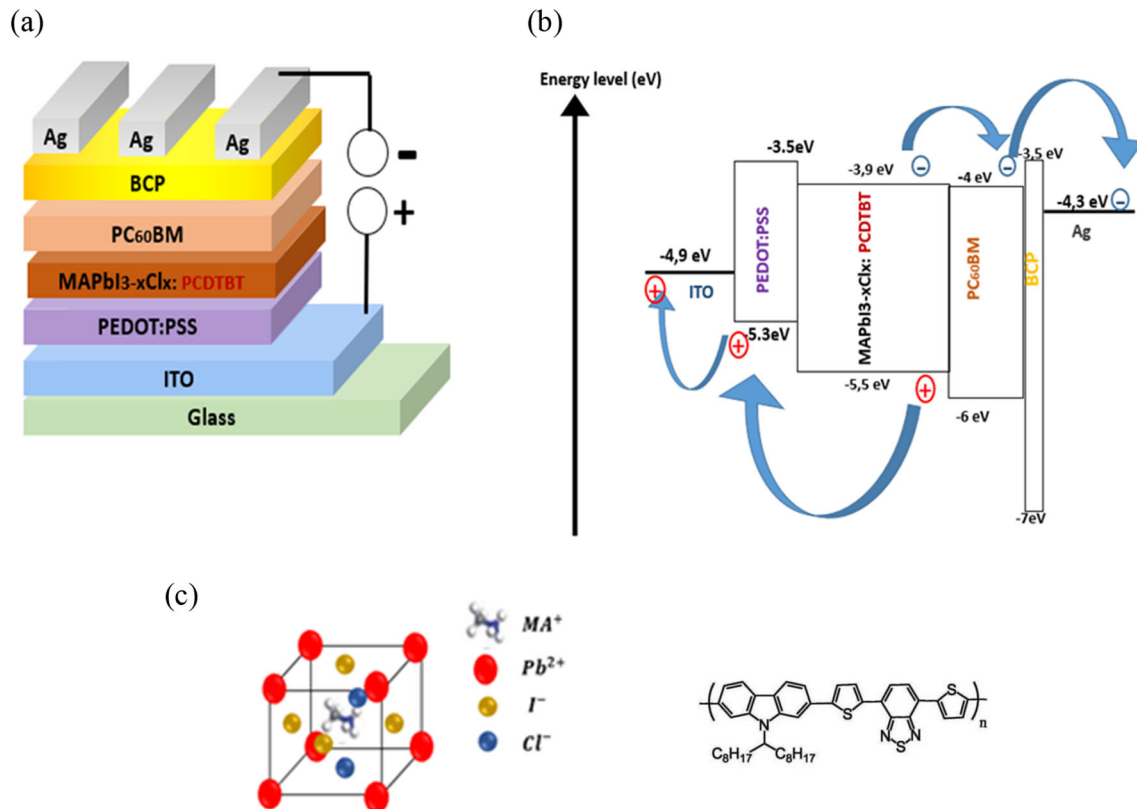
Fig. 1 (**a**) Structure of the device, (**b**) schematic energy-level diagram and (**c**) molecular structures of the mixed halide perovskite $MAPbI_{3-x}Cl_x$ and the PCDTBT

3 Results and discussion

3.1 Current density–voltage (J–V) characteristics

Two cells configurations, ITO/PEDOT: PSS/$MAPbI_{3-x}Cl_x$/$PC_{60}BM$/BCP/Ag and the ITO/PEDOT: PSS/$MAPbI_{3-x}Cl_x$ + PCDTBT/$PC_{60}BM$/BCP/Ag, were characterized. The selected J–V curves of the devices are presented in Fig. 2, while the extracted photovoltaic parameters are summarized in Table 1.

According to the present studies, the cell performances were improved by the addition of PCDTBT, the efficiency increasing with more than 2% (9.3% of the $MAPbI_{3-x}Cl_x$ vs. 11.6% of the mixed cell with mixed absorber layer). This improvement is the consequence of the enhancement of all the photovoltaic parameters, including Voc, Jsc and FF.

The increases of V_{oc} from 0.89 V to 0.94 V and of the fill factor FF from 53% to 56% might be correlated with a reduced the charge recombination in the absorber layer. The short-circuit current density (J_{SC}) has increased from 19.60 mA/cm² to 21.83 mA/cm²,
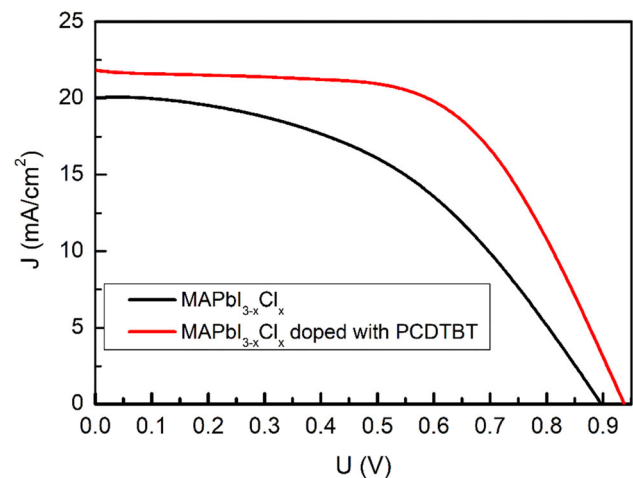

Fig. 2 Current density–voltage (J–V) characteristics of the $MAPbI_{3-x}Cl_x$-based solar cells with and without PCDTBT

which can be attributed also to a better light absorption in the perovskite doped with PCDTBT, as compared with the pure perovskite one.

Table 1 Photovoltaic performance of the best PSCs based on doped and undoped $MAPbI_{3-x}Cl_x$

Device	V_{OC} (V)	J_{SC} (mA/cm^2)	FF (%)	PCE (%)
$MAPbI_{3-x}Cl_x$	0.891	19.60	53	9.3
$MAPbI_{3-x}Cl_x$ doped 0.2 mg PCDTBT	0.940	21.83	56	11.6

3.2 UV–Vis spectra and luminescent properties

The optical properties of the absorber layers elaborated on ITO/Glass substrates are further examined. Figure 3a displays the UV–Vis absorption spectra for the doped and undoped films. It can be seen that all the perovskite thin films had a broad optical absorption range from 400 to 800 nm. All films showed a sharp absorption increase around 745 nm, corresponding to the bandgap transition [22, 23].

A second peak at 490 nm is associated to the direct optical transition of the iodinated lead octahedron PbI_6 [24].

As shown in the figures, the addition of the PCDTBT did not change the shape of the absorption spectrum of perovskite, but has significantly increased absorption intensity of the perovskite films in the 400–800 nm range, mainly due to PCDTBT addition and its strong absorption. Higher absorbance leads to more generated charges, which can boost the performances of the solar cell (Fig. 3).

The bandgap energy of the undoped and doped perovskite films was estimated from the Tauc plot curve (Fig. 4). The calculated gap values are 1.56 eV
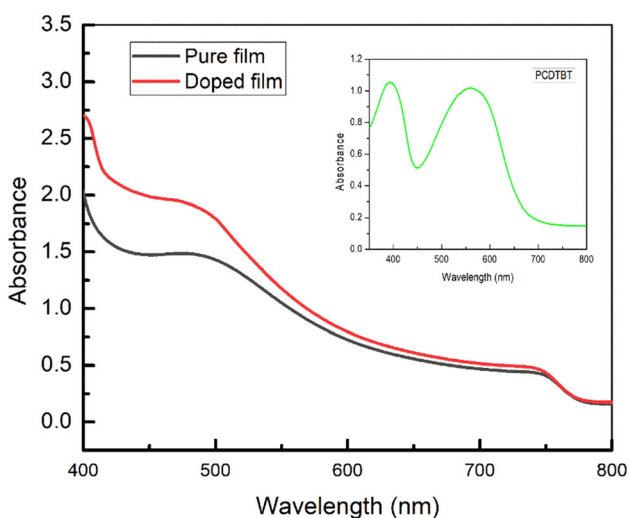
and 1.57 for the pure and doped perovskite, respectively. The energy gap has increased by PCDTBT doping which could contribute in the increase of open-circuit voltage.

In order to verify the effect of PCDTBT doping on the mechanism of the charge separation, a steady-state photoluminescence (PL) study was carried out.

Figure 5 presents the steady PL spectra of the perovskite films fabricated with and without PCDTBT. All the PL spectra show an emission peaks at 760 nm. These peaks show a slight shift towards the longest wavelength relative to the peak of the absorptions with a bandgap of 1.63 eV, which is known as the Stokes shift [25].

Further, as shown in Fig. 5, the undoped perovskite film presents the highest PL intensity, indicating the recombination of charge carriers in the perovskite film. On the other hand, since the doping of the PCDTBT to the perovskite, the intensity of the PL has been reduced, which clearly demonstrates the efficiency separation of the charge carriers and the fast transportation of the holes to the PEDOT:PSS layer that can minimize the recombination pathways due to passivation of the trap states of the perovskite layer [26, 27].

These results are explained by the good alignment of the energy levels of the highest occupied molecular orbit (HOMO) between the PEDOT:PSS (5.3 eV), PCDTBT (5.45 eV) and perovskite (5.5 eV).
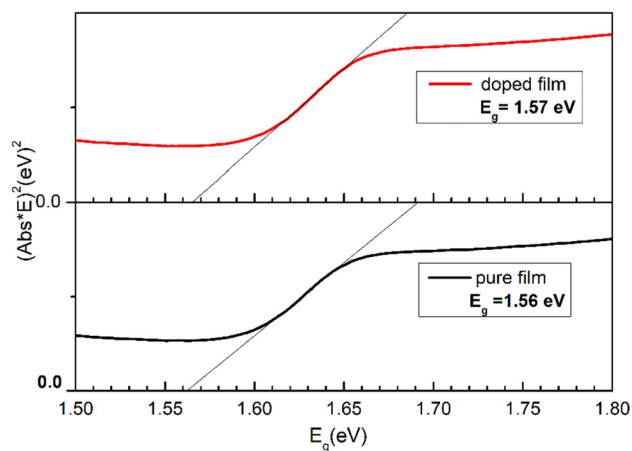
Fig. 3 **a** The absorption spectrum of films based on $MAPbI_xCl_{3-x}$: PCDTBT (0.2 mg mL^{-1}) and $MAPbI_xCl_{3-x}$ and **b** the absorption spectrum of PCDTBT (inset)

Fig. 4 Tauc plot of pure and doped perovskite
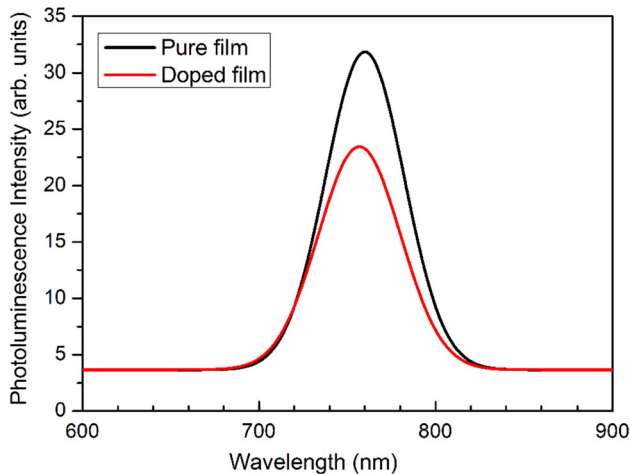
Fig. 5 PL spectra of films based on MAPbI$_x$Cl$_{3-x}$ with and without adding PCDTBT

Fig. 6 XRD patterns of the MAPbI$_{3-x}$Cl$_x$ perovskite films with and without PCDTBT

Furthermore, the PCDTBT has reacted as a good hole collector between the PEDOT:PSS and the perovskite layer. It extracts the holes in the perovskite layer towards the HOMO of the PEDOT:PSS, which led to the suppression of charge recombination and the increase of the PL intensity.

Adding PCDTBT to the perovskite solution can effectively passivate these traps and significantly reduce interface charge recombination, which stimulates the J$_{SC}$ and FF device. We can conclude that the addition of PCDTBT as doping material had improved the extraction and charge transfer from the perovskite absorber to the PEDOT:PSS before recombination at the interface. Besides, it can effectively passivate these hole traps and significantly reduce interface charge recombination, which stimulates the V$_{OC}$ device.

3.3 Perovskite thin-film structure: X-ray analyses

To gain insight into the effect of the PCDTBT additive on the crystal structure of the perovskite material, X-ray diffraction (XRD) data were collected for the diffraction patterns of the films. Figure 6 shows the XRD diagrams of the perovskite films deposited from MAPbI$_{3-x}$Cl$_x$ and MAPbI$_{3-x}$Cl$_x$ doped with PCDTBT precursor solution.

All the XRD patterns of the perovskite films show a tetragonal structure of the perovskite (MAPbI$_3$) with a characteristic peak located at 14.09°, 28.47°,31.71° and 43.29°, which are assigned separately to the (110), (220), (310) and (330) planes [28–30]. We note also the
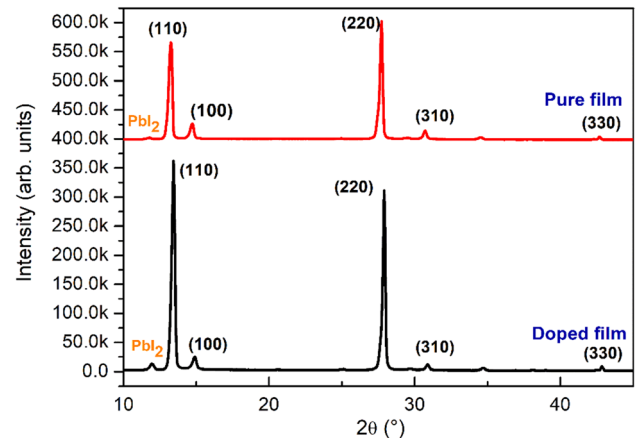
presence of a peak at 2Θ = 14.99°, corresponding to the plane (100) which is attributed to the pure chlorinated perovskite MAPbCl$_3$ [31]. A small peak at 12.45° is also marked which is attributed to the plane (001) of PbI$_2$. It should be noted that no PbCl$_2$ peak is observed in all the XRD spectra, indicating that the starting PbCl$_2$ precursor is completely consumed in reaction with MAI to form the MAPbI$_{3-x}$Cl$_x$.

It is clearly demonstrated that the addition of PCDTBT has caused an interesting effect on the diffraction patterns. This is observed by the increase of the intensity of the diffractions peak after the incorporation of the PCDTBT which clearly indicates a significant improvement in the degree of crystallinity of the perovskite film.

In order to better analyze the effect of the incorporation of PCDTBT, it is very interesting to evaluate the crystallinity of the samples over the full width at half maximum (FWHM) of characteristic diffraction peaks.

Thereby, the maximum values of full width at half maximum FWHM in the planes (110) were extracted from the X-ray diffraction patterns and their variations with and without the addition of PCDTBT are summarized in Table 2.

The value of the FWHM is 0.336° for pure MAPbI$_{3-x}$Cl$_x$, whereas this value has decreased to 0.293° after PCDTBT doping. Furthermore, a gradually and slightly broadened FWHM of XRD suggests that the crystallite sizes increase for the films doped with PCDTBT contents from 23.81 nm to 27.31 nm. These crystallite sizes for the main peak (110) were determined by Debye–Scherrer equation (Eq. 1) [32].

Table 2 The full width at half maximum (FWHM) of (110) diffraction peak extracted from the XRD patterns

Sample	FWHM
$MAPbI_{3-x}Cl_x$	0.336
$MAPbI_{3-x}Cl_x$ doped 0.2 mg PCDTBT	0.293

$$L = \frac{K\lambda}{\beta \cos\Theta},\qquad(1)$$

where L is the average crystallite size, λ is the X-ray wavelength in nanometer (nm), β is the peak width of the diffraction peak profile at half maximum height resulting from small crystallite size in radians and K is a constant related to crystallite shape, normally taken as 0.9.

Indeed, the FWHM is a good sense for the existence of defects formed in the semiconductor layer and usually, the existence of crystalline defects causes the widening of the FWHM peak and conversely [33].

A moderate excess of PbI_2 in the doped perovskite film is noted. The ratio calculation of PbI_2 relative to the amount of MAPI is in order of 0.035 and 0.0175 for pure and doped perovskite, respectively. According to the literature, the presence of PbI_2 is beneficial as a passivation of defects [34].

Hence, the XRD analyses have demonstrated that the incorporation of PCDTBT has improved the perovskite film crystallinity, which subsequently has reduced the default that can cause the charge recombination.

3.4 Scanning electron microscopy

Figure 7 shows the SEM images of the $MAPbI_{3-x}Cl_x$ films deposited on ITO substrate covered by a PEDOT:PSS layer in top view of surface, with and without the PCDTBT addition.

Both samples show a uniform, compact film with full surface coverage. The perovskite film consists of grains with sizes around 200 nm which are closely related (Fig. 2a). When 2 mg of PCDTBT was added in the perovskite precursor, there was a remarkable change in the film morphology in terms of grain size and coverage of film (Fig. 2b). We can observe that the PCDTBT was distributed in the final film and the grain size of the perovskite film has increased after it was added. In fact, the grains become larger with a crystallite around 300–400 nm which could be attributed to better crystallization of the perovskite layer. This enhancement of the grain size can affect the carrier mobility and the charge recombination which led to higher efficiency.

Thus, we can note the presence of more grains with a slight contrast in the grain boundaries, which is consistent with the enhancement of the PbI_2 intensity phase in the XRD measurement.

3.5 Hysteresis effect

A slight hysteresis phenomenon was seen for the device with the doped perovskite. Figure 8 shows the J–V plots of the solar cell with doped perovskite measured in opposite scan directions and the extracted parameters are summarized in Table 3.
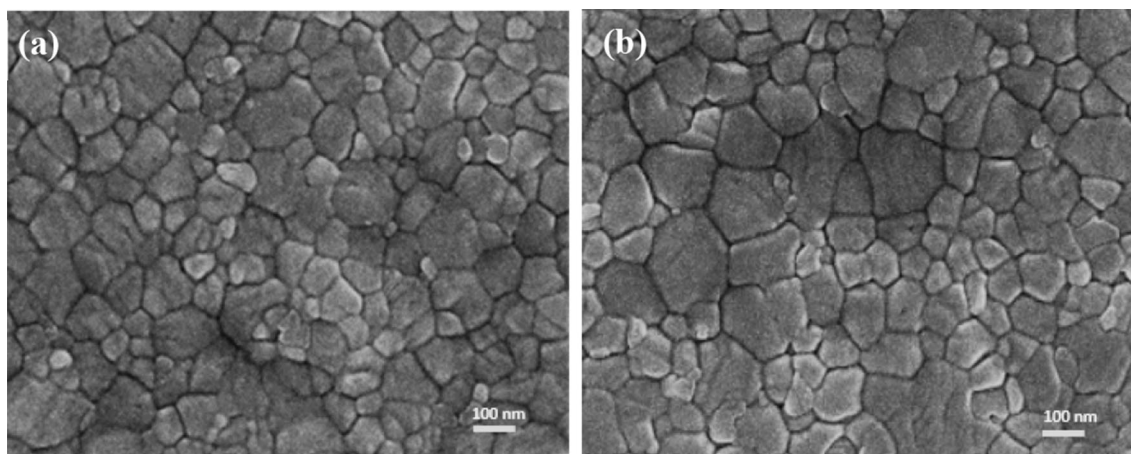

Fig. 7 The top SEM morphology images of perovskite crystal films with different concentrations of PCDTBT; (**a**) CH3NH3PbI$_{3-x}$Cl$_x$, (**b**) CH3NH3PbI$_{3-x}$Cl$_x$: PCDTBT (0.2 mg mL^{-1})
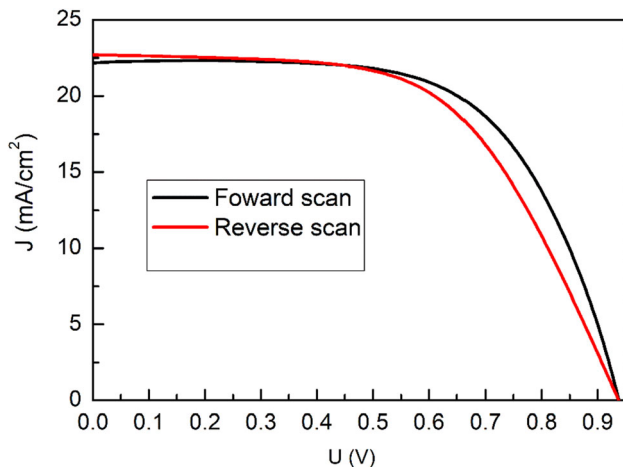
Fig. 8 J–V plots of solar cell using the perovskite doped with PCDTBT with forward and reverse

Table 3 Photovoltaic performance of PSC based on doped MAPbI3-xClx with forward and reverse scan

Device	V_{OC} (V)	J_{SC} (mA/cm^2)	FF (%)	PCE (%)
Forward scan	0.940	21.83	56	11.6
Reverse scan	0.934	21.54	54	10.8

This cell achieves a PCE of 11.6% with a V_{OC} of 0.940 V, a J_{SC} of 21.83 mA/cm^2, and a FF of 56% when measured under forward voltage scan and a slight lower PCE of 10.8% with a V_{OC} of 0.934 V, a J_{SC} of 21.54 mA/cm^2, and an FF of 54% for the reverse scan. This small hysteresis can be attributed to various physical causes such the presence of a high density of defects inside or on the surface of the material [35–37].

4 Conclusion

In summary, inverted perovskite solar cells based on MAPbI$_{3-x}$Cl$_x$ with and without PCDTBT as doping materials were fabricated. It was shown that the PCDTBT additive can effectively increase the device performance. It can greatly facilitate the crystallization process of the perovskite film and effectively minimize the charge carrier's recombination owing to the interface created between PCDTBT and the perovskite. As a result, the PCDTBT-based doped device has shown significantly improved performance than the undoped perovskite devices. Finally, we have

successfully achieved a PCE of 11.6% with a Jsc of 21.83 mA/cm^2, a V_{OC} of 0.940 V and a FF of 56%.

Data availability

All data generated or analyzed during this study are included in this published manuscript.

Compliance with ethical standards

Conflict of interest   There are no conflicts of interest to declare.

References

1. H. Tan, A. Jain, O. Voznyy, et al., Science **355**(6326), 722–726 (2017). https://doi.org/10.1126/science.aai9081
2. Y. Lv et al., RSC Adv. **8**(37), 20982–20989 (2018). https://doi.org/10.1039/c8ra03559h
3. R. Lindblad et al., Phys. Chem. C **119**(4), 1818–1825 (2015). https://doi.org/10.1021/jp509460h
4. J. Niu et al., Org. Electron. **48**, 165–171 (2017). https://doi.org/10.1016/j.orgel.2017.05.044
5. L. Xiao et al., Org. Electron. **50**, 33–42 (2017). https://doi.org/10.1016/j.orgel.2017.07.020
6. W.S. Yang et al., Science **356**(6345), 1376–1379 (2017). https://doi.org/10.1126/science.aan2301
7. A. Kojima et al., Am. Chem. Soc. **131**(17), 6050–6051 (2009). https://doi.org/10.1021/ja809598r
8. https://www.nrel.gov/pv/cell-efficiency.html
9. H. Mehdi, M. Muriel, et al., Mater. Sci. Mater. Electron., 1–9 (2020). https://doi.org/10.1007/s10854-020-03571-9
10. S. Ye et al., Nano Lett. **15**(6), 3723–3728 (2015). https://doi.org/10.1021/acs.nanolett.5b00116
11. H. Mehdi et al., RSC Adv. **9**(23), 12906–12912 (2019). https://doi.org/10.1039/c9ra02036e
12. I.M. Dharmadasa et al., Mater. Sci. Mater. Electron. **30**(2), 1227–1235 (2019). https://doi.org/10.1007/s10854-018-0390-5
13. D.G. Lee et al., Appl. Surf. Sci. **477**, 131–136 (2019). https://doi.org/10.1016/j.apsusc.2017.11.124
14. A. Mhamdi et al., Thin Solid Films **690**, 137567 (2019). https://doi.org/10.1016/j.tsf.2019.137567

15. H. Mehdi, A. Mhamdi, et al., Physica E Low Dimens. Syst. Nanostruct. **119**(114000) (2020). https://doi.org/10.1016/j.physe.2020.114000

16. Y. Wu et al., ChemSusChem **11**(5), 837–842 (2018). https://doi.org/10.1002/cssc.201702221

17. M. Saliba et al., Science **354**(6309), 206–209 (2016). https://doi.org/10.1126/science.aah5557

18. W. Rehman et al., Energy Environ. Sci. **10**(1), 361–369 (2017). https://doi.org/10.1039/c6ee03014a

19. H. Mehdi, A. Mhamdi, et al., Mater. Sci. Semicond. Process. **109**, 104915 (2020). https://doi.org/10.1016/j.mssp.2020.104915

20. N.D. Pham et al., Mater. Chem. A **5**(10), 5195–5203 (2017). https://doi.org/10.1039/c6ta11139d

21. https://www.ossila.com/products/pcdtbt?fbclid=IwAR3ypJd04pNtQ5gNMWAmzcyXp0lvzayTYGyNWk9S4VwEIWhLIWIJzNyAFnw&variant=20202368897

22. G. Maculan et al., Phys. Chem. Lett. **6**(19), 3781–3786 (2015). https://doi.org/10.1021/acs.jpclett.5b01666

23. S. Jin et al., Power Sources **404**, 64–72 (2018). https://doi.org/10.1016/j.jpowsour.2018.10.008

24. B.-w. Park et al., Chem. Mater. **26**(15), 4466–4471 (2014). https://doi.org/10.1021/cm501541p

25. R. Albani, *Principles and Applications of Fluorescence Spectroscopy* (Wiley, Chichester, 2008)

26. S. Gamliel et al., Phys. Chem. C **119**(34), 19722–19728 (2015). https://doi.org/10.1021/acs.jpcc.5b07554

27. Y. Yuan et al., Nat. Mater. **10**(4), 296 (2011). https://doi.org/10.1038/NMAT2951

28. Y. Deng et al., Energy Environ. Sci. **8**(5), 1544–1550 (2015). https://doi.org/10.1039/c4ee03907f

29. Y. Zhou et al., Mater. Chem. A **3**(17), 9249–9256 (2015). https://doi.org/10.1039/c4ta07036d

30. C. Sun et al., Phys. Chem. C **120**(24), 12980–12988 (2016). https://doi.org/10.1021/acs.jpcc.6b05255

31. T. Baikie et al., Mater. Chem. A **3**(17), 9298–9307 (2015). https://doi.org/10.1039/c5ta01125f

32. Y. Liu et al., Appl. Surf. Sci. **410**, 241–248 (2017). https://doi.org/10.1016/j.apsusc.2017.03.085

33. M. Vashista et al., Philos. Mag. **92**(33), 4194–4204 (2012). https://doi.org/10.1080/14786435.2012.704429

34. H. Xu et al., Phys. Chem. Chem. Phys. **18**(27), 18607–18613 (2016). https://doi.org/10.1039/c6cp02737g

35. A. Mhamdi et al., Mol. Struct. **1192**(1–6), 1–6 (2019). https://doi.org/10.1016/j.molstruc.2019.04.113

36. F. Wu et al., ACS Appl. Mater. Interfaces **10**(30), 25604–25613 (2018). https://doi.org/10.1021/acsami.8b07298

37. F. Wu et al., ACS Energy Lett. **3**(10), 2457–2460 (2018). https://doi.org/10.1021/acsami.8b07298

⚛ Springer